MYO1A (Brush Border Myosin I) Dynamics in the Brush Border of LLC-PK1-CL4 Cells

M. J. Tyska* and M. S. Mooseker*†‡
Departments of *Molecular, Cellular, and Developmental Biology, †Cell Biology, and ‡Pathology, Yale University, New Haven, Connecticut 06520 USA

ABSTRACT The kidney epithelial cell line, LLC-PK_1-CL4 (CL4), forms a well ordered brush border (BB) on its apical surface. CL4 cells were used to examine the dynamics of MYO1A (M1A; formerly BB myosin I) within the BB using GFP-tagged MIA (GFP-M1A), MIA motor domain (GFP-MDIQ), and tail domain (GFP-Tail). GFP-β-actin (GFP-Actin) was used to assess actin dynamics within the BB. GFP-M1A, GFP-Tail, but not GFP-MDIQ localized to the BB, indicating that the tail is sufficient for apical targeting of M1A. GFP-Actin targeted to all the actin domains of the cell including the BB. Fluorescence recovery after photobleaching analysis revealed that GFP-M1A and GFP-Tail turnover in the BB is rapid, ~80% complete in <1 min. As expected for an actin-based motor, ATP depletion resulted in significant inhibition of GFP-M1A turnover yet had little effect on GFP-Tail exchange. Rapid turnover of GFP-M1A and GFP-Tail was not due to actin turnover as GFP-Actin turnover in the BB was much slower. These results indicate that the BB population of M1A turns over rapidly, while its head and tail domains interact transiently with the core actin and plasma membrane, respectively. This rapidly exchanging pool of M1A envelops an actin core bundle that, by comparison, is static in structure.

INTRODUCTION

The brush border (BB) domain found on the apical surface of intestinal and renal proximal tubule epithelial cells provides an excellent model system for studying the organization of the actin cytoskeleton and its interaction with the plasma membrane (reviewed in Mooseker, 1985; Coudrier et al., 1988; Bement and Mooseker, 1996). Composed of large arrays of microvilli (MV), the BB exhibits one of the most highly ordered arrays of filamentous actin observed in nature. MV in these arrays are nearly identical in length and diameter, each containing a single actin bundle polarized so that all barbed (plus) ends extend into the tip of a given MV. The filaments of these bundles are cross-linked together by villin, fimbrin, and espin (Bartles et al., 1998). The bundle is tethered to the MV membrane by ezrin (Algrain et al., 1993; Berryman et al., 1993) and, in the intestinal BB, a periodically spaced spiral array of bridges composed of the class I myosin, MYO1A (M1A, formerly BB myosin I; reviewed in Mooseker and Cheney, 1995; Coluccio, 1997). Similar bridges have also been described in the rat renal BB and may be in part composed of M1A (Coluccio, 1991).

Given the well-ordered nature of the cytoskeleton found within the BB, questions arise as to how cells maintain and regulate the size and shape of these structures. Currently, except for measurements of protein degradative turnover (Stidwill et al., 1984; Stidwill and Burgess, 1986), there are no data regarding the dynamics of the cytoskeletal components of the BB. Here we explore the dynamics of M1A. M1A is of particular interest because it is an actin-based molecular motor, with the potential to be regulated by the chemical and mechanical environment within the MV.

The ~110-kDa heavy chain of M1A consists of three functionally distinct domains. These include an N-terminal motor domain, a neck domain consisting of at least three IQ motifs, each of which binds a calmodulin light chain (CaM), and a basic tail that may act as a membrane binding domain via interaction with acidic phospholipids. The enzymatic, mechanochemical and structural properties of M1A (purified from chicken BBs) have been extensively analyzed. M1A is a slow, plus-end-directed motor (~60 nm/s at room temperature) and exhibits complex regulation of its ATPase activity by Ca^{2+} through its CaM light chains (reviewed in Mooseker and Cheney, 1995; Coluccio, 1997).

Transient kinetics studies on M1A have revealed that the rates of certain biochemical transitions in the M1A ATPase cycle diverge from those measured for myosin II. Slow rates of ADP release and ATP-induced dissociation result in a longer strongly bound lifetime (>50 ms) relative to myosin II (<5 ms) (Cooke, 1997; Jontes et al., 1997). However, because the steady-state turnover rate is also slow (Jontes et al., 1997), the probability of existing in the strongly bound state (i.e., the duty ratio) is still low (~5–10%), similar to that of myosin II (Harris and Warshaw, 1993). Both cryo-EM data (Jontes et al., 1995; Jontes and Milligan, 1997) and single-molecule measurements (Veigel et al., 1999) suggest that the M1A may be designed to generate tension for extended periods and not for powering rapid movement along actin. Similar properties have been observed for myr-1 (Myo1b) and smooth muscle myosin II (Cremo and Geeves, 1998; Coluccio and Geeves, 1999).

Currently, there is no clear understanding of M1A function. Hypotheses regarding M1A function include a struc-

Submitted November 21, 2001, and accepted for publication January 18, 2002.

Address reprint requests to Dr. Matthew J. Tyska, 342 Kline Biology Tower, 266 Witney Ave., Department of Molecular, Cellular, and Developmental Biology, Yale University, New Haven, CT 06520. Tel.: 203-432-3469; Fax: 203-432-6161; E-mail: matthew.tyska@yale.edu.

0006-3495/02/04/1869/15 $2.00

tural role in tethering the actin core to the membrane, buffering of intramicrovillar Ca^{2+} via its CaM light chains, and mechanochemical facilitation of nutrient or electrolyte absorption either through a stirring mechanism or through regulation of specific membrane transporters. An active role in movement of newly synthesized apically targeted membrane vesicles to the BB membrane has also been proposed (Fath and Burgess, 1994). The closely related myosin-Iα (Myo1b) has been shown to associate with endosomal vesicles (Raposo et al., 1999). Moreover, expression of truncated forms of MIA disrupts the distribution and function of the endosomal compartment (Durrbach et al., 1996, 2000).

We assessed the intramicrovillar dynamics of M1A using the BB-expressing cell line, LLC-PK_1-CL4 (CL4). CL4 cells properly target GFP-tagged M1A to their BB surface. Because they contain particularly long MV (up to 4 μm) compared with other BB-expressing cell lines, these cells also allow visualization of M1A dynamics along the long axis of the MV. By performing fluorescence recovery after photobleaching (FRAP) experiments on GFP-M1A expressed in CL4 cells, we show that ~80% of the population of M1A exchanges rapidly. Similar measurements with GFP-tagged β-actin show that the actin core in these BBs turns over at a much slower rate relative to M1A, indicating that treadmilling of this microfilament population cannot account for the rapid rate of exchange observed for M1A. To understand which subdomains of M1A are critical for its localization and dynamic behavior, truncated fusion proteins missing either the N-terminal motor domain or the C-terminal tail region were examined. These data reveal the C-terminus of M1A is necessary for proper M1A targeting and that this domain is influential in determining the kinetics of M1A turnover.

MATERIALS AND METHODS

Cell culture and drug treatments

CL4 cells (a gift from Carolyn Slayman, Yale University) were maintained as previously described (Hasson and Mooseker, 1994). For experiments involving live cell imaging, maintenance medium was replaced with imaging medium: base-DEM (dye free, Sigma Chemical Co., St. Louis, MO) supplemented with 5 mM D-glucose and 10 mM HEPES, pH 7.1. For drug treatments, maintenance medium was replaced with imaging medium plus inhibitors, and cells were incubated for 30 min before imaging. ATP depletion was accomplished by addition of 0.05% sodium azide and 10 mM 2-deoxy-D-glucose (Sigma) to glucose-free imaging medium (Nehls et al., 2000).

Cloning of GFP fusion constructs

Full-length and truncated GFP-M1A fusion proteins were assembled using standard molecular biological techniques. The full-length human M1A cDNA described by Skowron et al. (1998) was used as a template for all polymerase chain reactions (PCRs) described below. PCR (Expand, Roche Diagnostics, Indianapolis, IN) was performed with primers to introduce *Sac*I and *Xma*I restriction sites into the 5′ and 3′ ends of the full-length M1A cDNA, respectively. This cDNA (encoding amino acids (aa) 1–1043) was ligated into the polylinker of pEGFP-C1 (Clontech, Palo Alto, CA) in frame with the N-terminal EGFP coding sequence, creating the plasmid pGFP-MIA. To create a fusion protein lacking the C-terminal tail of M1A (aa 1–765, MDIQ), pGFP-M1A was digested with *Sac*I and *Ssp*I, creating a fragment that was ligated back into the *Sac*I and *Xma*I sites of the pEGFP-C1 polylinker. To fuse GFP to the C-terminal tail of M1A (aa 772-1043, Tail), PCR was used to create a fragment with 5′ *Xho*I and 3′ *Xma*I sites that allowed for ligation into the pEGFP-C1 polylinker. The EGFP-β-actin clone was a generous gift of Michael Way (EMBL, Heidelberg, Germany).

Transfections

CL4 cells at 70–80% confluency were transfected with Lipofectamine 2000 (GibcoBRL, Gaithersburg, MD) using the manufacturer's instructions. Forty-eight hours after transfection, cells were replated at limiting densities and grown in maintenance medium supplemented with 1 mg/ml G418 (GibcoBRL). Stable transformants were selected and sorted to enrich for the fluorescent cell population using fluorescence-activated cell sorting.

Antibodies

The following antibodies and corresponding dilutions were used for immunoblotting: anti-human M1A tail polyclonal antibody (Skowron et al., 1998), 2 μg/ml; anti-GFP polyclonal (Molecular Probes, Eugene, OR), 1 μg/ml; anti-villin monoclonal (Mab; AMAC, Westbrook, ME), 1:2000; anti-non-muscle myosin-II polyclonal (BTI), 1:1000; CX-1, a Mab raised against chicken M1A that recognizes the head domain of multiple myosins (Carboni et al., 1988; Peterson and Mooseker, 1992), 1:100 dilution of ascites fluid; anti-fimbrin polyclonal, 10 μg/ml (Peterson and Mooseker, 1992); anti-CaM Mab (Upstate Biotechnology, Lake Placid, NY), 1 μg/ml.

SDS-PAGE and immunoblotting

Protein fractions were analyzed with SDS-PAGE using 5–20% gradient gels. For immunoblotting, gels were transferred to nitrocellulose (80 V, 3.5 h). For CaM blots, gels were transferred onto polyvinylidene fluoride (30 V, 30 min) and processed by the method of Sacks et al. (1991). Immunogens were visualized using the ECL method according to the manufacturer's instructions (Amersham Pharmacia Biotech, Piscataway, NJ).

Cell fractionation and biochemical extraction

To isolate CL4 BBs, confluent cells were rinsed three times with Tris-buffered saline at 37°C, scraped from the flasks, and pelleted (1500 $\times$ *g*, 10 min). Subsequent steps were performed at 4°C. Cells were resuspended in 9 pellet volumes of BB homogenization buffer (4 mM EDTA, 1 mM EGTA, 1 mM dithiothreitol (DTT), 1 mM Pefabloc, 20 mM imidazole, pH 7.2) and then lysed with a dounce. The extent of lysis was monitored by light microscopy. The homogenate was spun at 15,000 $\times$ *g* for 10 min. The resulting pellet (P1) contained BBs, as well as MV, and was the source of material for further experiments. For light microscopy, P1 was resuspended in BB homogenization buffer with or without 40 nM rhodamine-phalloidin (Molecular Probes) and allowed to incubate on ice for 2 h before imaging. For biochemical extractions, P1 was resuspended in extraction buffer (75 mM KCl, 1 mM EGTA, 2.5 mM $MgCl_2$, 1 mM DTT, 1 mM Pefabloc, 20 mM imidazole, pH 7.2) supplemented with one or more of the following: 1% Triton X-100, 1 mM MgATP, or 500 mM KCl. Extractions were incubated on ice for 20 min and then spun at 15,000 $\times$ *g* for 10 min. After removing the supernatant, the pellet was resuspended, boiling SDS-PAGE sample buffer was added, and samples were then processed for electrophoresis and immunoblotting.

Immunoprecipitation

GFP-M1A fusion protein was immunoprecipitated from CL4 lysates as follows. Cell pellets were obtained as above; all subsequent steps were performed at 4°C. Cells were resuspended in 9 pellet volumes of M1A solubilization buffer (150 mM KCl, 1% Triton X-100, 4 mM $MgCl_2$, 2 mM ATP, 1 mM EGTA, 1 mM DTT, 1 mM Pefabloc, 20 mM imidazole, pH 7.2) and lysed with a dounce. Lysates were spun at 50,000 × *g* for 20 min and the supernatant was precleared with 1% protein-A Sepharose (PAS; Amersham Pharmacia Biotech) for 1 h with gentle rocking. PAS beads and antibodies (100 μg/ml; nonimmune IgG (Jackson Immunoresearch, West Grove, PA) or anti-GFP (Clontech)) were added to the supernatant, and the mixture was incubated overnight with gentle rocking. PAS beads were then pelleted and washed several times with wash buffer (150 mM KCl, 1 mM EGTA, 0.5% Triton X-100, 2 mM $MgCl_2$, 1 mM DTT, 1 mM ATP, 1 mM Pefabloc, 20 mM HEPES, pH 7.2) and then prepared for SDS-PAGE and immunoblotting.

Light microscopy

Phase-contrast and fluorescent images of isolated BBs were acquired on a Nikon Diaphot 300 inverted microscope using a Zeiss 63×/1.4/Ph3 Plan Apochromat lens. Phalloidin staining for visualization of F-actin in fixed cells expressing GFP constructs was performed as described in Hasson and Mooseker (1994). Digital images (512 × 480 pixels × 8 bits) were acquired with a Photometrics (Tucson, AZ) ImagePoint cooled CCD under control of the Metamorph software package (Universal Imaging Corp., Downingtown, PA). Images were calibrated, pseudo-colored, and overlaid using Metamorph. All confocal images were acquired on a Bio-Rad (Richmond, CA) MRC-1024 laser scanning confocal microscope using a Zeiss 100×/1.4/DIC Plan Apochromat objective. Still images of live cells in the plane parallel to the coverslip surface (*x-y*) were acquired by Kalman averaging three to five scans with the scan rate to normal. Vertical sections (*z*) were scanned with resolution set to high, *z*-step interval of 0.37 μm, and scan rate set to normal. Two-color images of fixed cells (GFP, rhodamine-phalloidin) were acquired with sequential scanning.

FRAP experiments

FRAP experiments were performed on a Bio-Rad MRC-1024 laser scanning confocal microscope. FRAP experiments on other non-epithelial cell types have been performed with the intent of imaging the entire thickness of the specimen (low-NA objective, pinhole fully opened) (Hirschberg et al., 1998). In contrast, the experiments reported here were performed with a high-NA lens (Zeiss 100×/1.4 Plan Apochromat) and the confocal pinhole closed down (4 mm) to limit fluorescence contributions from regions outside of the BB (e.g., the underlying cytosol). For these studies, CL4 cells were grown in collagen-coated glass-bottom 35-mm culture dishes (Willco Wells, Amsterdam, The Netherlands) for 1 week after confluency. Dishes with confluent monolayers were mounted on the microscope in a dish warmer (Warner Instruments, Hamden, CT) at 37°C. For FRAP experiments with MV perpendicular to the focal plane, the Bio-Rad time course module was used to select a region of interest (ROI) for bleaching that occupied ~6.25 μm^2 (2.5 × 2.5 μm) in a field of 11,556 μm^2 (107.5 × 107.5 μm). This corresponded to <5% of the apical surface from a single cell in the *x-y* plane (~100–150 μm^2). Bleaching was accomplished by zooming the laser (10× zoom, 30% transmission) and scanning the ROI three times with the scan rate set to normal. Immediately after zooming and bleaching, the entire field was scanned (1× zoom, 30% transmission) and this image was taken as $t = 0$. FRAP in the ROI was monitored by scanning the entire field once every 3 s with scan rate set to normal. Both bleaching and recovery scan parameters were chosen to minimize photodamage of the specimen. Metamorph was used to extract the ROI integrated pixel intensity values from Bio-Rad movie stacks and export them to a Microsoft Excel spreadsheet where background and the $t = 0$ intensity value were subtracted from each time point. Intensity values were normalized so that the scan immediately before the bleach was set equal to 1, and all subsequent ROI intensity values were expressed relative to this pre-bleach value. Normalized recovery curves from a number of cells and monolayers were then averaged. To extract rate and mobile fraction parameters for relative comparison between constructs and drug treatments, TableCurve 2D (SPSS) was used to fit the averaged data to the following expression:

$$I_{ROI}(t \geq 0) = \alpha - A_1 \exp^{-k_1 t}(- A_2 \exp^{-k_2 t}), \qquad (1)$$

where, I_{ROI} is the ROI intensity at time $t \geq 0$, α is the mobile fraction, A_1 is the amplitude of the exponential process with rate k_1 and is equal to the α in the absence of the second process (enclosed in parentheses). In this general model, A_1 is related to the fraction of the total population that exchanges at rate k_1. Data were fit with and without the second exponential process, and the goodness of each fit was judged by the amplitude and randomness of residuals.

Imaging and FRAP were also performed on MV that were parallel to the focal plane. The bleached ROI for these experiments ranged from 4 to 16 μm^2. The pre-bleach and post-bleach recovery scans were taken at 2× zoom (30% transmission; pinhole, 4 mm) to enable the visualization of fine structure. Because the higher zoom resulted in significant photobleaching during recovery scans, these data were used strictly for qualitative assessments and were not curve fit for rate or mobile fraction determination.

Online supplemental material

Four QuickTime movies of the FRAP experiments shown in Figs. 6 and 9 are available online.

RESULTS

Characteristics of CL4 brush borders

Brush borders, morphologically similar to those isolated from proximal tubules (Kenny and Booth, 1978) were isolated from differentiated CL4 monolayers using the same fractionation methods developed for isolation of BBs from enterocytes (Fig. 1 *A*) (Mooseker and Howe, 1982). Comparable to renal BBs, CL4 BBs possessed MV ranging in length from ~2.5 to 4 μm and contained the MV core proteins villin and fimbrin and the subapical component, myosin II (Fig. 1 *B*) (Coudrier et al., 1988). These BBs also contained several immunogens of 110–130 kDa, revealed with the monoclonal antibody CX-1 (Fig. 1 *B*) (Carboni et al., 1988), that are likely to be class I myosins given their M_r. CX-1, raised against chicken M1A, is reactive with an epitope near the ATP binding site of M1A and also reacts with numerous other myosins including human M1A (Peterson and Mooseker, 1992). The anti-human M1A (Skowron et al., 1998) also recognized an ~110-kDa immunogen. However, the biochemical extraction profile of this protein was very different from M1A and other endogenous myosins (see below), suggesting that this may simply represent cross-reactivity with another non-myosin BB component.

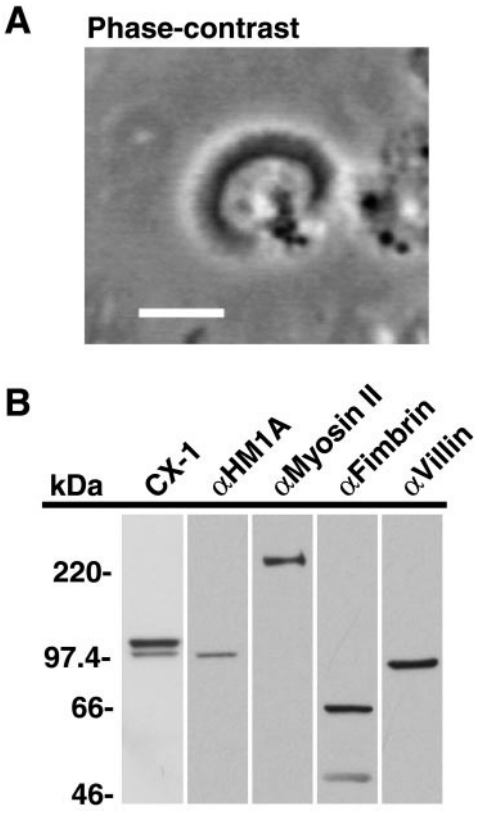

FIGURE 1 CL4 BB characteristics. (*A*) Phase-contrast image of an isolated BB from a CL4 cell. Bar, 5 μm. (*B*) Immunoblots probing the subcellular fraction enriched in BBs with CX-1, anti-(α) HM1A (110 kDa), αVillin (95 kDa), αFimbrin (68 kDa), and α-non-muscle myosin-IIa (220 kDa). The lower M_r band appearing in the anti-fimbrin blot is most likely the product of proteolysis.

GFP-tagged proteins are stably expressed in CL4 cells

Cell homogenates from four stably transfected CL4 cell lines (GFP-M1A, GFP-MDIQ, GFP-Tail, and GFP-Actin; Fig. 2 *A*) were probed with anti-GFP, revealing that each expressed GFP-immunogens of the expected M_r (~145 kDa for GFP-M1A, ~114 kDa for GFP-MDIQ, ~57 kDa for GFP-Tail, and ~70 kDa for GFP-Actin; Fig. 2 *B*).

Localization of GFP-tagged proteins

Confocal light microscopy revealed that GFP-M1A localized to the BB and lateral membrane, mirroring the expression profile of M1A in the enterocyte (Fig. 3 *A*) (Peterson and Mooseker, 1992; Heintzelman et al., 1994; Skowron et al., 1998). GFP-Actin, localized to all the actin-containing domains of the cell, including the BB, junctional margins, and lateral membranes (Fig. 3 *D*). In contrast to GFP-M1A, GFP-Actin also assembled into stress fibers (Fig. 3 *E*).

Of the two M1A truncations, only GFP-Tail demonstrated localization similar to the full-length construct (Fig. 3 *C*). GFP-MDIQ exhibited a diffuse pattern of fluorescence and had a dramatic effect on monolayer morphology including a marked decrease in monolayer height (Fig. 3 *B*). To further characterize the localization of these fusion proteins, we fixed confluent monolayers and stained the actin cytoskeleton with phalloidin. Confocal sections through the apical BB domain revealed significant overlap between the native actin signal (red) and both GFP-M1A and GFP-Tail (green; Fig. 4, *A* and *C*). Although GFP-MDIQ-expressing cells possessed MV on their apical surface, the GFP signal did not extend significantly into these structures (Fig. 4 *B*). When the basal surfaces of the same phalloidin-stained monolayers were examined, there was little or no colocalization of GFP-M1A, GFP-MDIQ, or GFP-Tail with stress fibers (data not shown). A similar result has been reported for human M1A in Caco-2_{BBE} cells (Skowron et al., 1998).

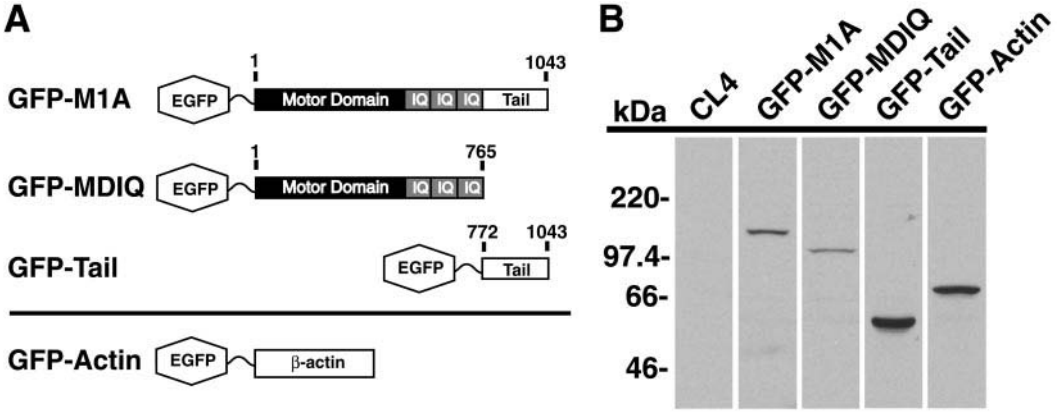

FIGURE 2 Expression of GFP-tagged proteins in CL4 cells. (*A*) Schematic representation of the EGFP fusion constructs used for transfection in this study. Numbers indicate relevant amino acids with 1 = the N-terminus of M1A. (*B*) Whole-cell homogenates probed with αGFP. All four stable lines expressed GFP-immunogens of the expected M_r.

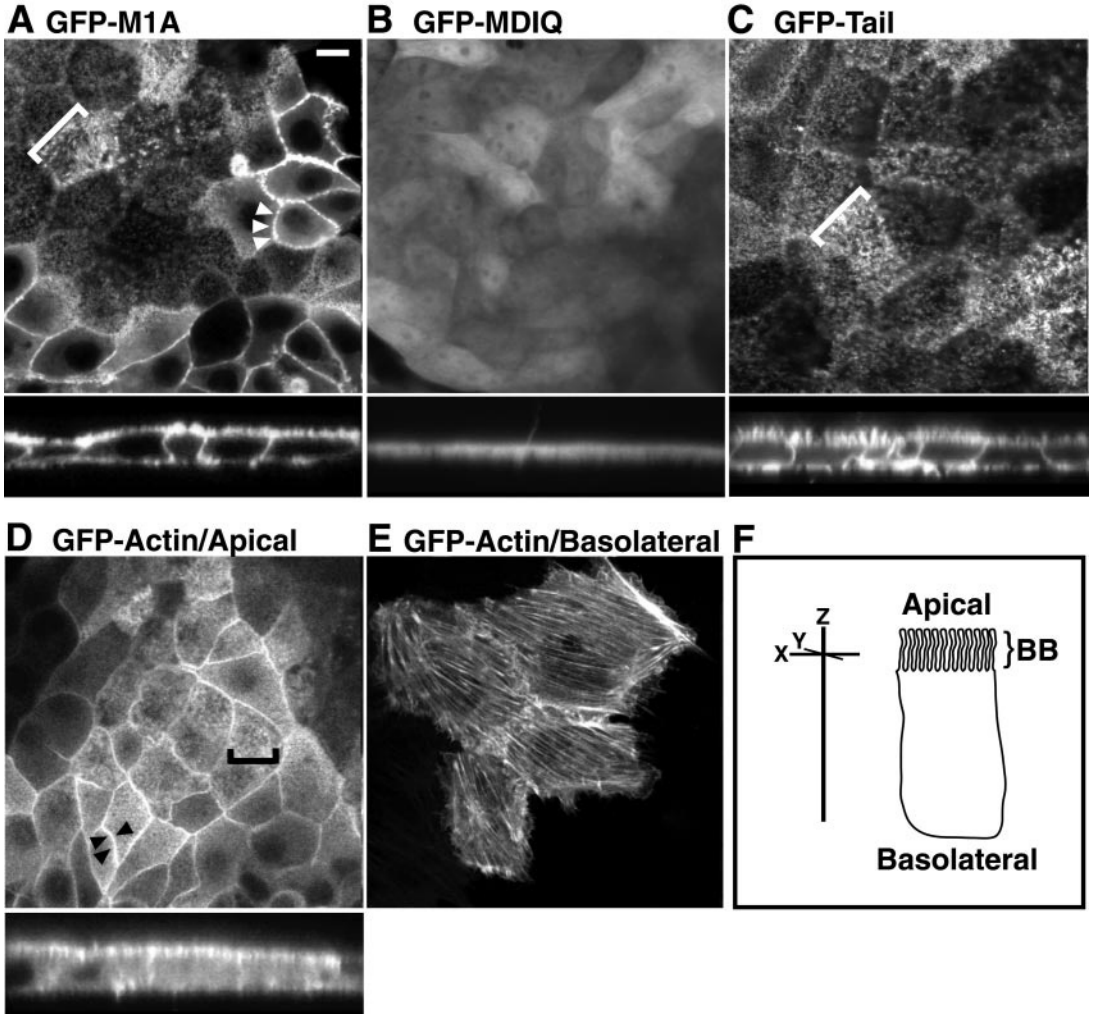

FIGURE 3 Confocal sections of live CL4 cells expressing GFP-tagged proteins. The localization of GFP-M1A (*A*), GFP-MDIQ (*B*), GFP-Tail (*C*), and GFP-Actin (*D*) in the BBs of live confluent monolayers. En face confocal sections are shown with a representative vertical section below each panel (*A–D*). GFP-M1A, GFP-Tail, and GFP-Actin localize to the BB, whereas GFP-MDIQ does not. Brackets in *A*, *C*, and *D* are positioned to highlight MV signal. Arrowheads in *A* and *D* are positioned to highlight lateral localization. Incorporation of GFP-Actin into stress fibers can be seen in *E*, where the basolateral surface of a partially differentiated cell island is shown. (*F*) A polarized epithelial cell with corresponding three-dimensional orientation as designated in this study. Bar, 10 μm.

GFP-M1A demonstrates characteristics similar to native M1A

To establish whether GFP-M1A expression was producing a fully functional fusion protein, several assays were performed to probe for characteristics of M1A. GFP-M1A was purified by immunoprecipitation (IP) from extracts of isolated BBs treated with detergent, high salt, and ATP. Immunoblot analysis of IP-purified GFP-M1A confirmed the presence of CaM (Fig. 5 *A*). Densitometric analysis of stained protein gels of these IP preparations (Fig. 5 *B*) revealed a molar ratio of ~3.5:1 (CaM:GFP-M1A), comparable to that of purified M1A (Wolenski et al., 1993).

A hallmark feature of the association state of M1A with BBs isolated from human enterocytes and Caco-2_{BBE} cells is that a combination of detergent, salt, and ATP is required for complete solubilization (Carboni et al., 1987; Peterson and Mooseker, 1992; Skowron et al., 1998). Comparable results were observed for the solubilization of GFP-M1A from isolated CL4 BBs. After mechanical lysis of CL4 cells, GFP-M1A remained associated with the BB-containing pellet fraction in a manner similar to other endogenous BB-associated myosins (see Fig. 5 *C*, CX-1 panel). Although significant release of GFP-M1A from Triton- or salt-treated BBs occurred following the addition of ATP, complete solubilization of GFP-M1A required detergent treatment, ATP, and high salt (Fig. 5 *D*). The extraction properties demonstrated by GFP-M1A appeared identical to those demonstrated by other endogenous BB-associated myosins (Fig. 5 *D*, CX-1 panel). These results indicate that GFP-M1A, like M1A and other myosins in the human enterocyte

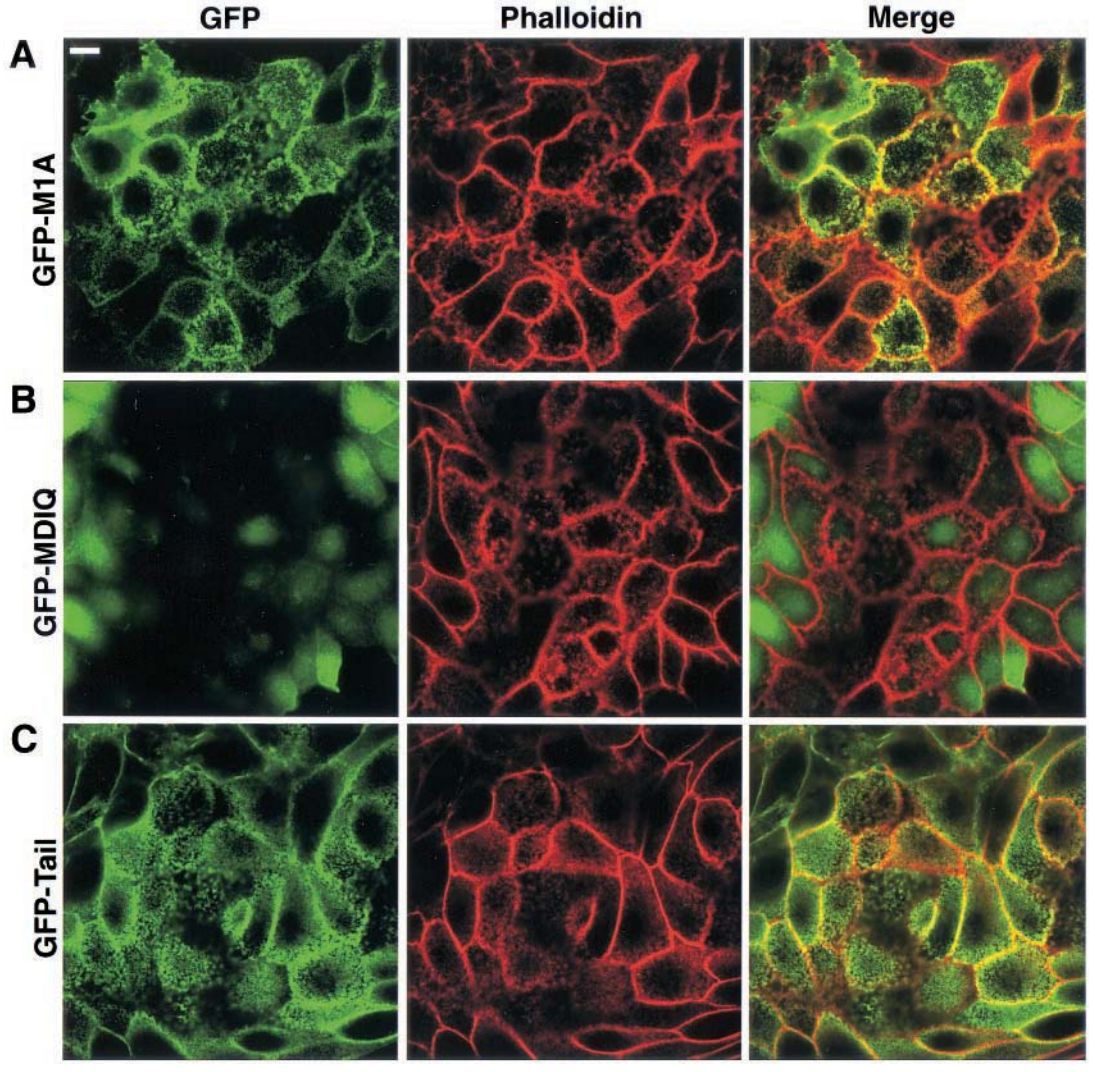

FIGURE 4 Apical confocal sections of phalloidin-stained CL4 monolayers. Colocalization of the GFP and phalloidin signals from confluent monolayers expressing GFP-M1A (*A*), GFP-MDIQ (*B*), and GFP-Tail (*C*). Overlays are shown in the merge panels. Bar, 10 μm.

BB recognized by the CX-1 antibody (Peterson and Mooseker, 1992), is tightly associated with the BB through both ATP-dependent and ATP-independent, salt-sensitive interactions. In contrast, the endogenous ~110-kDa immunogen recognized by anti-M1A (but not CX-1) was completely released by detergent alone (data not shown), suggesting that it may not represent a myosin.

Phase-contrast and fluorescence light microscopy were used to examine isolated BBs following fractionation. Consistent with the biochemical studies above, these BBs retained GFP-M1A signal that overlapped with F-actin (Fig. 5 *E*). ATP extraction of these (membrane-intact) BBs resulted in disordering of the MV and partial loss of the GFP signal with the remaining fluorescence in small, irregularly shaped patches (Fig. 5 *F*).

FRAP analysis reveals rapid turnover of GFP-M1A and GFP-Tail within the brush border

Performing FRAP analysis on cells expressing GFP-tagged proteins can reveal information regarding the turnover kinetics of the labeled population, as well as the fraction of the population that participates in turnover (mobile fraction, α) (Axelrod et al., 1976). To quantify the recovery process, FRAP data can be fit to mathematical models that allow the extraction of one-dimensional diffusion coefficients (Cole et al., 1996; Nehls et al., 2000). The application of these models to this work is complicated by several factors, including the columnar cell shape and highly convoluted nature of the BB observed in confluent CL4 monolayers. Moreover, because GFP-M1A is a motor, models that describe passive diffusion may not accurately fit data where

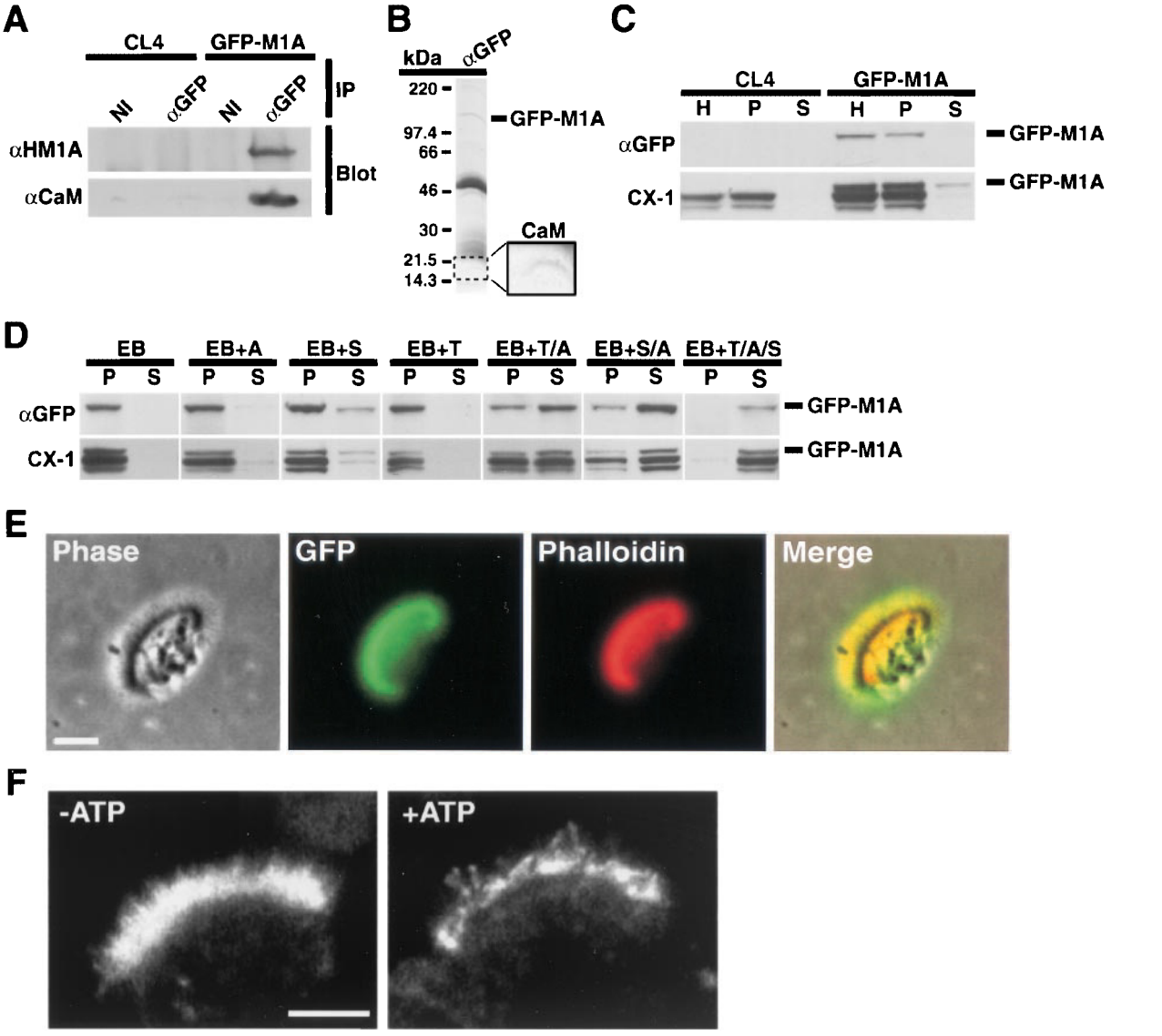

FIGURE 5 Examining GFP-M1A for native characteristics. (*A*) IP of GFP-M1A from either CL4 parent cells or cells stably expressing GFP-M1A using an αGFP or non-immune IgG (NI). Immunoblots with αHM1A and αCaM indicate that CaM co-immunoprecipitates with the fusion protein. (*B*) Protein-stained gel of immunoprecipitated GFP-MIA; densitometry revealed a GFP-M1A:CaM ratio of ~1:3.5. (*C*) Immunoblots (probed with αGFP or CX-1) of whole-cell homogenates (H) of CL4 or GFP-M1A-expressing cells and supernatant (S) and pellet (P) fractions following a 15,000 × *g* spin. (*D*) Extraction of BB-enriched fractions in either extraction buffer alone (EB) or EB supplemented with one or more of the following: 1% Triton (T), 1 mM ATP (A), and 0.5 M KCl (S). (*E*) Phase contrast and fluorescence light microscopy of a rhodamine phalloidin-stained isolated BB from a GFP-M1A cell. Merge panel shows the overlap of the phase image with the GFP and phalloidin signals. (*F*) Confocal image showing a single GFP-M1A containing BB before (−ATP) and after ATP extraction (+ATP). Bars, 5 μm.

active processes (e.g., directed movement) may contribute to the observed response (Axelrod et al., 1976). To avoid these complications, we fit average recovery curves for each construct to a general kinetic model (Eq.1), enabling the estimation of rates of recovery and the mobile fraction.

When FRAP was performed on small patches of MV in the BBs of confluent GFP-M1A cells, the recovery of fluorescence was rapid, ~80% complete after 1 min (Figs. 6 *A* and 7 *A*). Recovery data averaged over all bleach runs for GFP-M1A was best fit with two kinetic components (Materials and Methods, Eq.1). In the case of GFP-M1A, the fast and slow processes had rates of 0.132 s^{-1} and 0.026 s^{-1}, respectively, and demonstrated roughly equal amplitudes (Fig. 7, *D* and *E*, and Table 1). The sum of the amplitudes from both processes equals α, in this case 0.77. The recovery demonstrated by GFP-Tail appeared similar yet slightly faster (Fig. 6 *C*), and the resulting curve (Fig. 7 *B*) was also best fit with two components. Here, the fast and slow processes had rates of 0.252 s^{-1} and 0.035 s^{-1}, again with roughly equal amplitudes and

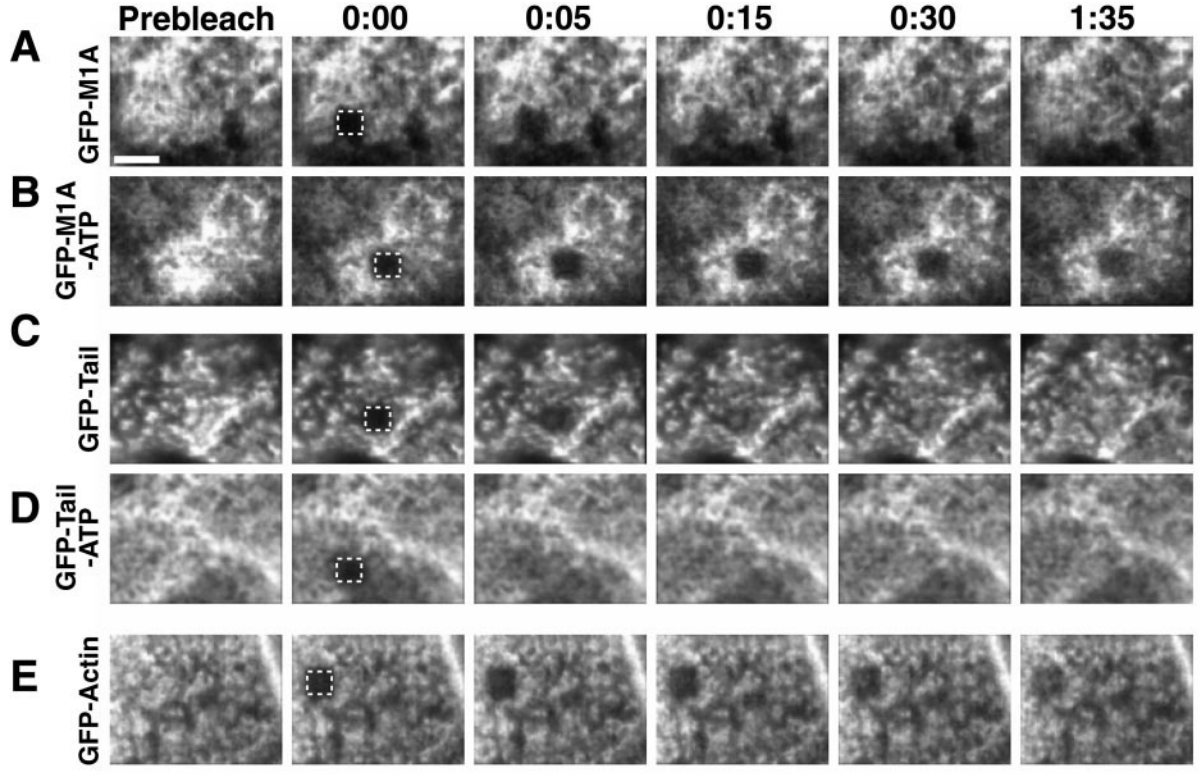

FIGURE 6 FRAP analysis in the *x-y* plane of the monolayer. Montage panels show a single frame before photobleaching (prebleach) and a five-frame time series subsequent to the bleach pulse for GFP-M1A (*A*), GFP-M1A plus 0.05% sodium azide/10 mM 2-deoxy-D-glucose (*B*), GFP-Tail (*C*), GFP-Tail plus 0.05% sodium azide/10 mM 2-deoxy-D-glucose (*D*), and GFP-Actin (*E*). The dashed square indicates the bleached region in the $t = 0$ frame, an area of ~6.25 μm^2. Bar, 5 μm.

α of 0.91 (Fig. 7, *D* and *E*, and Table 1). Thus, the observation of faster recovery for GFP-Tail can be explained by the initial rapid phase being ~2-fold faster than that observed for GFP-M1A.

Given that MV GFP-M1A binds to the underlying actin core, the rapid turnover of this motor may be related to the treadmilling of actin in these structures. Likewise, the turnover of GFP-Tail could also be limited by actin dynamics if its localization within the MV is restricted by the endogenous population of myosins I or other membrane-microfilament linkers bound to the actin core. To determine whether the turnover kinetics of GFP-M1A and GFP-Tail are related to the turnover of MV actin, the BBs of cells expressing GFP-Actin were also probed with FRAP (Fig. 6 *E*). GFP-Actin recovery (Fig. 7 *C*) was best fit to two exponential processes with fast and slow rates of 0.232 s^{-1} and 0.006 s^{-1} (Fig. 7 *D* and Table 1). The amplitudes for these rates were 0.12 and 0.40, respectively, providing α of 0.52 (Fig. 7 *E* and Table 1). The dominant slow component and significantly lower α indicate that although BB actin does turn over, the process is too slow to account for the turnover kinetics observed for GFP-M1A and GFP-Tail.

FRAP of GFP-M1A is inhibited by cellular ATP depletion

In cells depleted of ATP (0.05% sodium azide, 10 mM 2-deoxy-D-glucose; (Nehls et al., 2000), turnover of GFP-M1A was greatly suppressed (Fig. 6 *B*, dashed line in Fig. 7 *A*). Slight recovery did take place, however, and the curve was best fit to a single process with a rate of 0.028 s^{-1} and a low α of 0.19 (see Table 1). As expected for a fusion protein lacking a motor domain, ATP depletion had little impact on the turnover of GFP-Tail (Fig. 6 *D*, dashed line in Fig. 7 *B*).

During ATP depletion, any soluble GFP-M1A should become strongly bound to a permissive actin population (e.g., the MV core). The limited FRAP observed under conditions of ATP depletion could be related to the slow detachment of rigor-bound GFP-M1A or to some other ATP-independent process (e.g., GFP-M1A tail binding within MV). To determine whether rigor-bound GFP-M1A detaches and redistributes in the time frame of these experiments, we performed FRAP on the tips of MV from isolated BBs under rigor conditions (Fig. 8, *A* and *B*), allowing observation of any redistribution in GFP-M1A signal without the influence of a soluble pool. There was no redistribution of GFP-M1A in the

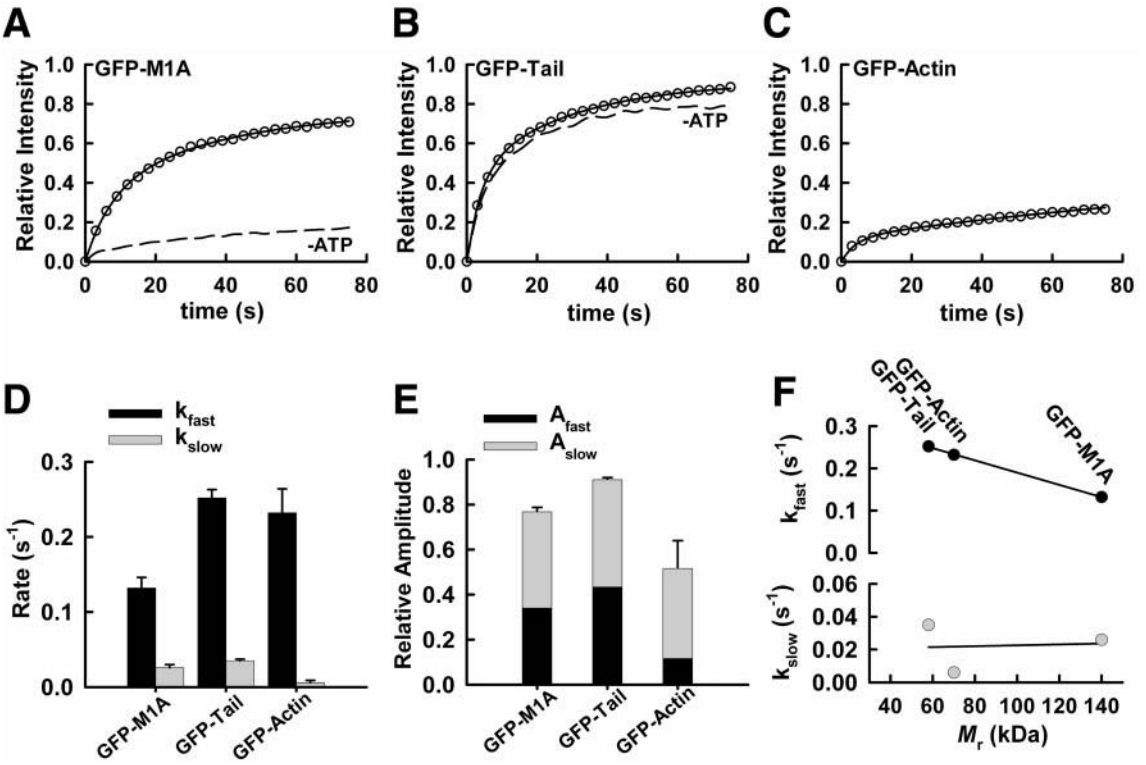

FIGURE 7 FRAP data and analysis. Plots show data for GFP-M1A (*A*), GFP-Tail (*B*), and GFP-Actin (*C*). In each plot, the open circles represent the average recovery of multiple runs. In *A* and *B*, the dashed black line (−ATP) represents the recovery observed in ATP-depleted cells. (*D*) A summary plot of the rate constants from the curve fits in *A–C* (fast phase, black; slow phase, gray). (*E*) A summary plot of the amplitude data from the curve fits in *A–C* (fast phase, black; slow phase, gray). In this stack representation, the vertical height of each bar (the sum of slow and fast amplitudes) represents the total mobile fraction in each case. The difference between the value at the top of the bar and 1.0 represents the immobile fraction in each case. (*F*) A scatter plot indicating that the rate of the initial rapid phase of fluorescence recovery correlates well with the M_r of each construct, whereas the slow phase does not.

time frame of these observations. Assuming that the BB is saturated with rigor-bound GFP-M1A when the FRAP experiments are performed, the slight recovery observed in ATP-depleted cells is likely due to the soluble fraction of GFP-M1A that interacts with the BB in an ATP-independent manner.

Fluorescence recovers from MV base to tip for GFP-M1A and GFP-Tail but not GFP-Actin

Due to the uneven geometry of the CL4 monolayer, it was possible to image MV that were parallel to the focal plane during some experiments, allowing FRAP analysis in a plane parallel to the *z*-axis of the cell (Fig. 9 *A*; see Fig. 3 *F* for orientation). This analysis demonstrated that FRAP of GFP-M1A in the *z*-axis advanced from MV base to tip. Interestingly, the base-to-tip migration of GFP-M1A recovery was not motor domain driven as GFP-Tail recovery demonstrated similar, albeit more rapid, vectorial movement (Fig. 9 *B*).

The base-to-tip recovery observed for GFP-M1A and GFP-Tail makes intuitive sense given that the tube-like MV structure is open to the unbleached cytosolic pool at its base. However, similar experiments with GFP-Actin indicated that this is not the default result for MV proteins. Although the turnover of GFP-Actin in the BB of confluent monolayers demonstrated slow kinetics and a low mobile fraction

TABLE 1 FRAP data summary

Construct	*n*	k_{fast} (s^{-1})	A_{fast}	k_{slow} (s^{-1})	A_{slow}	α	A_{slow}/a
GFP-M1A	22	0.13 ± 0.01	0.34 ± 0.04	0.026 ± 0.004	0.43 ± 0.03	0.77 ± 0.02	0.56
GFP-M1A (−ATP)	9			0.028 ± 0.002	0.17 ± 0.01	0.19 ± 0.01	0.89
GFP-Tail	24	0.25 ± 0.01	0.43 ± 0.01	0.035 ± 0.002	0.48 ± 0.01	0.91 ± 0.01	0.53
GFP-Actin	16	0.23 ± 0.03	0.12 ± 0.01	0.006 ± 0.003	0.40 ± 0.11	0.52 ± 0.12	0.77

Values are fit parameter ± SE of the fit parameter. *n*, number of BBs sampled and included in the averaged curves; k_x, rate constant for process X; A_x, amplitude for process X; α, mobile fraction.

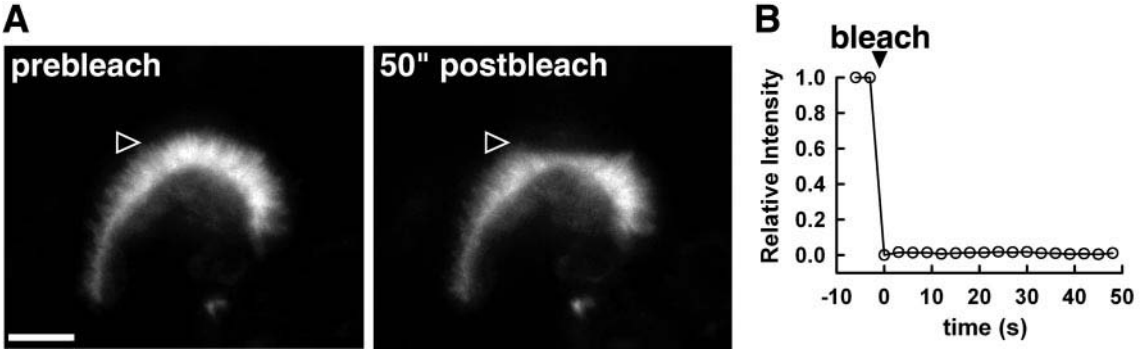

FIGURE 8 Confocal images showing FRAP analysis of an isolated BB under rigor conditions. (*A*) An isolated BB, before and after the bleach pulse, is shown with an arrowhead positioned adjacent to bleached region. Bar, 5 μm. (*B*) A trace of the fluorescence of the bleached region in *A*, immediately before and after the bleach pulse.

(see above), turnover in pre-confluent cells occurred on a time scale comparable to GFP-M1A and GFP-Tail. Strikingly, FRAP in these MV advanced from the tips down to the base (Fig. 9 *C*). The opposing polarity of GFP-M1A and GFP-Actin FRAP was clearly demonstrated when the ratio of tip-to-base intensity was plotted with respect to time (Fig. 10, *A* and *B*). FRAP analysis of GFP-Actin recovery in the *x-y* plane was not possible on these juvenile cells because of variability in MV length and density (compare Fig. 9, *A* and *B*, with *C*), presumably a reflection of the variety of differentiation states in these pre-confluent cultures.

DISCUSSION

CL4 cells as a model system for studying the BB cytoskeleton

The results presented here establish the CL4 line as an excellent model system for examining the dynamics of BB cytoskeletal proteins, including M1A. These cells form a well ordered, isolatable BB that is morphologically and compositionally comparable to those from the proximal tubule epithelial cell (Fig. 1). Several lines of evidence indicate that GFP-M1A expression mirrors that observed in vivo. The biochemical studies reported here demonstrate that GFP-M1A contains multiple CaM light chains. This critical finding demonstrates that there is sufficient endogenous CaM to provide the full complement of light chains required to support the enzymatic and actin-binding properties of GFP-M1A. Moreover, the extraction studies using isolated BBs indicate that the association state of human GFP-M1A with the BB is identical to that of M1A in isolated human BBs (Fig. 5). Most importantly, GFP-M1A properly targets to the apical BB surface of these cells (Figs. 3 *A* and 4 *A*).

Caco-2_{BBE} cells (Peterson and Mooseker, 1992, 1993; Peterson et al., 1993) are also well established as a BB model system. However, these cells possess very short MV in differentiated BBs ($\leq$1 μm in length), a characteristic that would greatly complicate FRAP analysis by reducing the fluorescence available from this domain (see Materials and Methods). CL4 BBs possess MV up to four times in length (Figs. 1 and 9, *A* and *B*), resulting in significantly greater BB signal. Nevertheless, using two-photon microscopy, Coscoy et al. (2001) have reported preliminary measurements of the dynamics of M1A and β-actin in Caco-2 cells that are qualitatively similar to the results presented here.

Localization of M1A in CL4 cells

The full-length construct, GFP-M1A, localized as expected in the BBs of differentiated cells (Figs. 3 *A* and 4 *A*). In addition to striking MV localization, GFP-M1A also associated with the lateral and basal plasma membrane (see vertical section in Fig. 3 *A*), a feature of M1A localization in vivo and in Caco-2_{BBE} cells (Heintzelman and Mooseker, 1990; Peterson and Mooseker, 1992; Skowron et al., 1998). However, in the intestine, levels of M1A staining on the basolateral margins of the enterocyte are much lower than at the apical surface, except for cells emerging from the crypt. Thus, the relatively high intensity of GFP-M1A fluorescence associated with the basolateral membrane of the CL4 cells may reflect the fact that these cells achieve a differentiation state equivalent to the partially differentiated state observed in intestinal crypt cells. Alternatively, the expression of GFP-M1A fusion protein in these cells is under the control of a powerful promoter (i.e., human cytomegalovirus) such that the labeling observed in the lateral and basal regions may represent secondary binding sites populated at high M1A concentrations.

Several studies have implicated M1A in vesicle trafficking (Fath and Burgess, 1994) and maintenance of membrane compartments (Durrbach et al., 1996, 2000). However, the low level of cytoplasmic GFP-M1A in CL4 cells is diffuse with no visible regions of concentration (Fig. 3 *A*). Although these data indicate that there is little steady-state

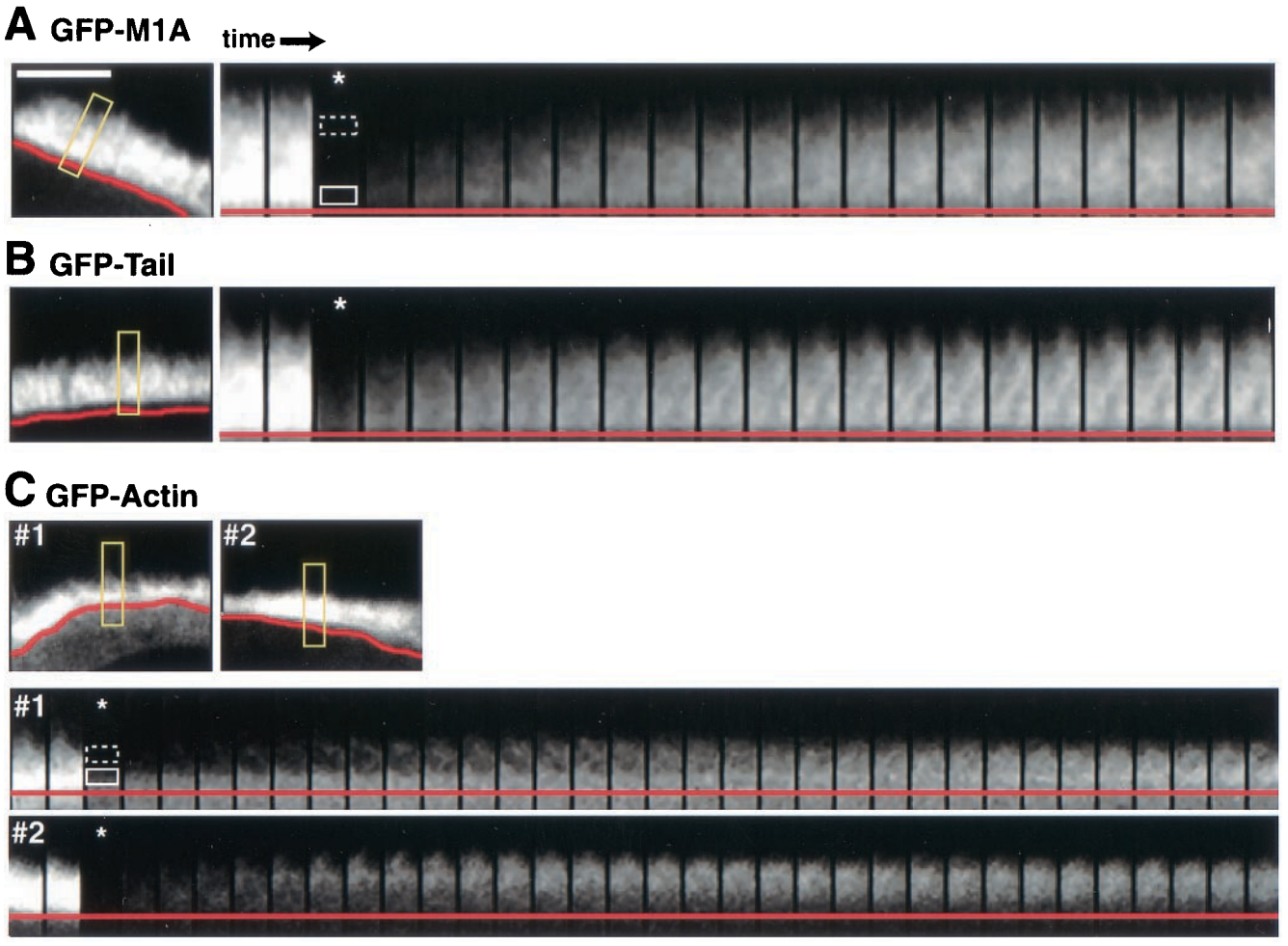

FIGURE 9 FRAP analysis along the *z*-axis of the BB. Montages show fluorescence recovery for GFP-M1A (*A*) and GFP-Tail (*B*) in fully differentiated monolayers, and two examples of GFP-Actin (*C*) in partially differentiated cells (where MV actin turnover is much faster). The first panel in each series shows the *z*-axis, lateral view of the MV before the bleach pulse. In *A*, *B*, and *C*, the yellow box highlights the region that was bleached and sampled for the accompanying montage. The frame marked with the white asterisk is $t = 0$. The superimposed red line in each series is drawn along the base of the MV. The solid and dashed white boxes in *A* and *C* denote the regions of the montages that were sampled for constructing the plots in Fig. 10. Time intervals are 5 s/frame for GFP-M1A and GFP-Actin and 3 s/frame for GFP-Tail.

organelle association with GFP-M1A in these cells, this result does not preclude the existence of GFP-M1A organelle interactions on a much more transient basis.

Domain-dependent localization

Of the two M1A truncations, GFP-Tail and GFP-MDIQ, only GFP-Tail localized in a manner similar to the full-length protein (Figs. 3 and 4). In contrast, GFP-MDIQ was diffuse throughout the cell and not excluded from the cytoplasm to the same extent as GFP-M1A or GFP-Tail. These data suggest that the lipid-binding domain found at the C-terminus of M1A contains enough targeting information to control the steady-state distribution of this molecular motor.

In contrast to the similar localization observed for GFP-M1A and GFP-Tail, experiments with full-length and truncated rat Myo1b suggest that the N-terminal motor domain of this myosin also plays a significant role in targeting full-length Myo1b to lamellapodia and other dynamic actin-containing structures (Ruppert et al., 1995; Tang and Ostap, 2001). More specifically, localization data obtained for a myosin II motor/Myo1b tail chimera suggests that the Myo1b motor domain may be involved in the selection of a specific subpopulation of microfilaments (Tang and Ostap, 2001). It follows that the M1A motor domain should contain similar targeting information. Why then does the GFP-MDIQ fusion protein demonstrate such gross mislocalization? Transient kinetic studies indicate that M1A is only strongly bound to actin for a small fraction of its ATPase

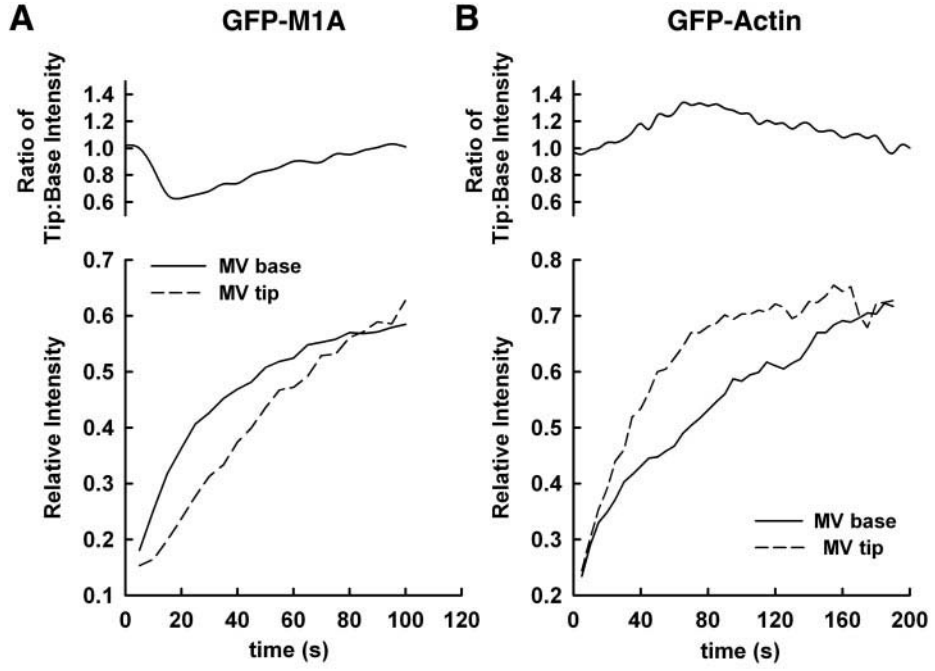

FIGURE 10 Plots showing the intensity changes over time at the base (——) and tip (— — —) regions of MV. Intensities forGFP-M1A (*A*) and GFP-Actin (*B*) were extracted from the corresponding solid and dashed line boxes drawn on the montages in Fig. 9, *A* and *C* (#1). Bar, 5 μm.

cycle (~5–10%; Jontes et al., 1997). Because the steady-state ATPase rate for M1A is rather slow at ~1 s^{-1} (Wolenski et al., 1993; Jontes et al., 1997), the detached period would last for an extended duration (~1 s), allowing the motor to diffuse away from actin. Thus, the diffuse GFP-MDIQ localization observed in this work may be due to the fact that the interaction with the BB actin population is too transient to influence the steady-state distribution of this fusion protein. Indeed, FRAP analysis of GFP-MDIQ revealed that this fusion behaved similarly to GFP alone, with recovery that was too fast to quantify with the confocal system used in these studies (results not shown). The targeting interaction involving the C-terminal tail region, potentially a direct interaction with the plasma membrane, dominates the steady-state distribution of M1A by localizing this protein during the extended period between actin interactions.

Intramicrovillar dynamics of M1A

FRAP analysis on cells expressing GFP-M1A, GFP-Tail, and GFP-Actin has enabled us to characterize the dynamics of these fusion proteins in the BB (Figs. 6 and 7). These results reveal that GFP-M1A demonstrates relatively high mobility while localized within the BB, a finding that requires modification of the historical view of M1A (based on ultrastructural studies) as a static structural microfilament-membrane linker. When similar analysis was performed on cells expressing GFP-Actin, this core protein also exhibited turnover, albeit to a limited extent and at a slower rate, indicating that actin treadmilling of the core bundle cannot account for the turnover of GFP-M1A. Moreover, FRAP experiments with GFP-Tail revealed a time course of fluorescence recovery comparable to that of GFP-M1A, suggesting the motor domain does not power the turnover of GFP-M1A.

A more quantitative view of the FRAP results was obtained by curve fitting the data with a general kinetic equation that makes no assumptions regarding cytoskeletal or membrane geometry (see Eq.1). Curve fits of FRAP data obtained for GFP-M1A, GFP-Tail, and GFP-Actin (Fig. 7, *A–C*) reveal a common feature: these data are all best fit with double-exponential functions. The most basic interpretation of this finding is that two populations contribute to the observed response.

Insight regarding the nature of the two populations comes from comparing the various constructs and treatments. Fig. 7 *F* reveals that the rate of the initial fast process observed for GFP-M1A, GFP-Tail, and GFP-Actin correlates well with the M_r of these fusion proteins, whereas the rate of the slow phase does not, suggesting that the initial phase might be diffusive in nature. If we make the assumption that M_r is proportional to the Stokes radius of each protein, then one would indeed predict that smaller proteins would take less time to diffuse the length of a given MV (see Howard, 2001). However, the transit time for proteins in this size range to diffuse a distance equal to the length of a MV would be predicted to be $\ll$1 s in a medium such as the

cytosol. The discrepancy between this prediction and the time constants determined by the fits here (4–7 s) may be related to the extremely high local viscosity of the intramicrovillar cytoplasm. Although there are currently no estimates of intramicrovillar viscosity, estimates of normal cytoplasmic viscosity indicate that this value is dependent on the size of the probing molecule but can be up to threefold higher than that measured for small proteins in water (Luby-Phelps et al., 1987).

Comparisons also help us define the second slow phase of FRAP. Intriguingly, the slower components of both GFP-M1A and GFP-Tail recovery are comparable in rate (~0.03 s^{-1}, Fig. 7 *D* and Table 1) and contribute to roughly half of the total recovery observed in each case (see A_{slow}/α in Table 1). ATP depletion of cells expressing GFP-M1A resulted in a recovery curve that was well fit by a single component with a rate similar to the slow phases observed for GFP-M1A and GFP-Tail (see Table 1). Given that the rate of the process in question is independent of the presence of a motor domain (GFP-Tail) or inhibition of the motor domain (GFP-M1A plus azide), we propose that this process represents the interaction between the M1A tail and the membrane.

The interpretation introduced above allows us to develop a model of the dynamic behavior of M1A and actin revealed by our FRAP observations. In the case of GFP-M1A, GFP-Tail, and GFP-Actin, the initial rapid phase of FRAP is likely driven by diffusion of unbound protein into and out of the MV. This process lasts only a few seconds as the intra-MV bleached population exchanges with the underlying cytosolic pool. The second slower phase may be governed by some capture mechanism that is related to how a specific protein is incorporated and/or retained within the BB. In the case of GFP-M1A and GFP-Tail, the capture mechanism could be the interaction between the tail and the membrane. However, in the case of GFP-Actin, this slow capture mechanism is likely an alternate process. The difference in capture mechanisms demonstrated by GFP-M1A/GFP-Tail and GFP-Actin is reflected in the differences of kinetics measured for the slow phases of these constructs (~0.005 s^{-1} for GFP-Actin vs. ~0.03 s^{-1} for GFP-M1A/GFP-Tail).

Experiments where FRAP was used to examine turnover in MV that were parallel to the focal plane (Fig. 9) provide additional evidence for distinct capture mechanisms for GFP-M1A/GFP-Tail and GFP-Actin. The *z*-axis FRAP examples given for GFP-M1A and GFP-Tail (Figs. 9, *A* and *B*, and 10 *A*) show that the front of fluorescence translates from MV base to tip during recovery. This would be the expected progression if unbleached protein diffused into the BB and was permitted to bind along the length of the MV. However, GFP-Actin FRAP in the MV of partially differentiated cells clearly migrates from tip to base (Figs. 9 *C* and 10 *B*). The deposition of GFP-Actin at MV tips before the sides or base strongly suggests that the capture mechanism that defines

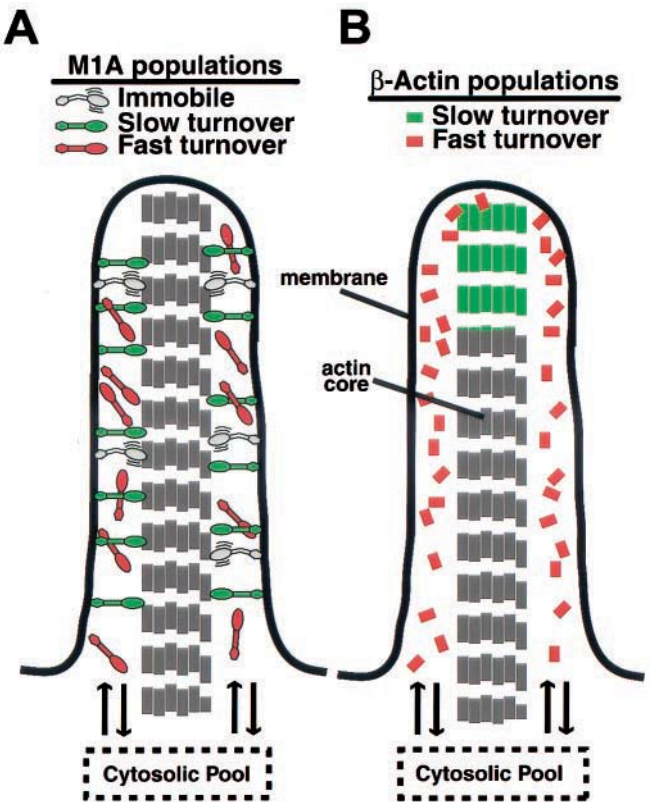

FIGURE 11 Models of M1A and β-actin turnover within the MV. (*A*) Three populations may contribute to the turnover observed for GFP-M1A: a rapidly exchanging population of M1A that is unbound (red), a slowly exchanging population that may represent M1A that is either head or tail bound (green), and perhaps a third population that does not turn over on the time scale of these observations (gray). This last population corresponds to the immobile fraction of ~0.2 and may represent motors that are trapped in a high force state. (*B*) Two populations may contribute to the turnover observed for GFP-Actin: a rapidly exchanging population of actin that is unbound or unincorporated (red) and a slowly exchanging population that may represent actin that becomes incorporated into the plus end of the MV actin bundle (green). Although curve fits to the FRAP data suggest a large immobile fraction for GFP-Actin, this is almost certainly an overestimate induced by the extremely slow rate of the second phase of recovery (0.005 s^{-1}).

the slow component observed for GFP-Actin in differentiated cells is plus-end incorporation into the core actin bundle. If we use the rate of the slow component of GFP-Actin recovery in differentiated cells (~0.005 s^{-1}) to estimate a rate of subunit incorporation into the core bundle, and assume that all filaments in the bundle incorporate at the same rate, we get a value (~0.3 s^{-1}) comparable to what one would expect for the steady-state flux of actin, i.e., treadmilling (Pollard and Mooseker, 1981). The rate estimated from the *z*-axis FRAP measurements on undifferentiated cells is roughly 10-fold faster (~3 s^{-1}), suggesting the presence of proteins that accelerate actin turnover (i.e., severing and capping proteins) in these immature microvilli.

The schematic models in Fig. 11 represent steady-state

snapshots of the various M1A and β-actin populations that may exist within a single MV as defined by our FRAP studies.

Role of the motor domain

Given the fact that GFP-Tail localizes and exchanges in a manner similar to GFP-M1A, questions arise as to the function of the motor domain during these dynamic processes. The findings presented in Fig. 5 indicate that the motor domain of the GFP-M1A fusion protein is properly folded and capable of interacting with actin in an ATP-dependent manner. Moreover, when the actomyosin interaction is perturbed with ATP depletion (Figs. 6 and 7), significant inhibition of FRAP is observed. The latter result indicates that although the motor domain is not necessary for turnover, it may be interacting with actin and generating force during the process. This possibility is supported by kinetic studies that show detachment of M1A from actin occurs at a rate of $\sim$20 s^{-1} (Jontes et al., 1997). The transient nature of the M1A-actin interaction would, therefore, not be expected to limit the turnover rates observed here ($\sim$0.13–0.03 s^{-1}). It is interesting to note that in CL4 cells expressing high levels of GFP-Tail, MV generally appeared longer and more irregular in length (compare vertical sections in Fig. 3, *A* and *C*). This may represent the dominant negative phenotype that results if this fragment competes for membrane binding sites with other endogenous membrane-microfilament cross-linkers within the MV. It is thus tempting to speculate that the M1A motor domain may play a role in regulating MV length by applying a force during its transient interaction with the actin core, pushing the bundle down into the cell. MV length would then be defined by the equilibrium established between the rate of plus-end actin incorporation and the minus-end-directed force generated by M1A.

Another intriguing aspect of the GFP-M1A FRAP data is that on the time scale of our measurements, $\sim$20% of the GFP-M1A does not exchange with the cytosolic pool. This small, immobile population may represent GFP-M1A molecules that are bound in a high-force state (Jontes et al., 1995; Jontes and Milligan, 1997), comparable to the latch state occupied by smooth muscle myosin (Cremo and Geeves, 1998). If this is the case, then the 20% immobile fraction may represent an in vivo determination of the high force duty ratio of this motor.

CONCLUSIONS

The dynamic nature of the BB cytoskeletal components reported here, and in particular the high mobility of M1A, requires modification of the longstanding belief that this highly organized domain becomes static following assembly. Future studies must focus on both the mechanism that cells employ to maintain such well-ordered structures in a dynamic state as well as the purpose of the dynamic state itself. From a regulatory standpoint, a dynamic cytoskeletal structure could allow for the alteration of the BB's physical properties (e.g., MV length, diameter, flexural rigidity, etc.) on a rapid time scale. This may represent a critical yet unexplored facet of the absorptive function of epithelial cells. The dynamic nature of M1A revealed in these experiments must also be combined with the abundance of in vitro biophysical data in the development of future functional hypotheses regarding this motor.

We thank Dr. Valerie Mermall for critical comments on the manuscript.

This work was supported by National Institutes of Health grants DK-25387 and DK-55389 to M.S.M. and DK-10113 (NRSA) to M.J.T.

REFERENCES

Algrain, M., O. Turunen, A. Vaheri, D. Louvard, and M. Arpin. 1993. Ezrin contains cytoskeleton and membrane binding domains accounting for its proposed role as a membrane-cytoskeletal linker. *J. Cell Biol.* 120:129–39.

Axelrod, D., D. E. Koppel, J. Schlessinger, E. Elson, and W. W. Webb. 1976. Mobility measurement by analysis of fluorescence photobleaching recovery kinetics. *Biophys. J.* 16:1055–69.

Bartles, J. R., L. Zheng, A. Li, A. Wierda, and B. Chen. 1998. Small espin: a third actin-bundling protein and potential forked protein ortholog in brush border microvilli. *J. Cell Biol.* 143:107–19.

Bement, W. M., and M. S. Mooseker. 1996. The cytoskeleton of the intestinal epithelium: components, assembly and dynamic rearrangements. *In* The Cytoskeleton., Vol. 3. I. F. Hesketh, editor. Jai Press, Greenwich, CT. 359–404.

Berryman, M., Z. Franck, and A. Bretscher. 1993. Ezrin is concentrated in the apical microvilli of a wide variety of epithelial cells whereas moesin is found primarily in endothelial cells. *J. Cell Sci.* 105:1025–43.

Carboni, J. M., K. A. Conzelman, R. A. Adams, D. A. Kaiser, T. D. Pollard, and M. S. Mooseker. 1988. Structural and immunological characterization of the myosin-like 110-kD subunit of the intestinal microvillar 110K-calmodulin complex: evidence for discrete myosin head and calmodulin-binding domains. *J. Cell Biol.* 107:1749–1757.

Carboni, J. M., C. L. Howe, A. B. West, K. W. Barwick, M. S. Mooseker, and J. S. Morrow. 1987. Characterization of intestinal brush border cytoskeletal proteins of normal and neoplastic human epithelial cells: a comparison with the avian brush border. *Am. J. Pathol.* 129:589–600.

Cole, N. B., C. L. Smith, N. Sciaky, M. Terasaki, M. Edidin, and J. Lippincott-Schwartz. 1996. Diffusional mobility of Golgi proteins in membranes of living cells. *Science.* 273:797–801.

Coluccio, L. M. 1991. Identification of the microvillar 110-kDa calmodulin complex (myosin-1) in kidney. *Eur. J. Cell Biol.* 56:286–294.

Coluccio, L. M. 1997. Myosin I. *Am. J. Physiol.* 273:C347–C359.

Coluccio, L. M., and M. A. Geeves. 1999. Transient kinetic analysis of the 130-kDa myosin I (MYR-1 gene product) from rat liver: a myosin I designed for maintenance of tension? *J. Biol. Chem.* 274:21575–21580.

Cooke, R. 1997. Actomyosin interaction in striated muscle. *Physiol. Rev.* 77:671–697.

Coscoy, S., F. Waharte, C. Brown, M. Arpin, P. Mangeat, E. Coudrier, and F. Amblard. 2001. Cytoskeletal dynamics of the apical membrane of epithelial cells: a two-photon FRAP study of the brush border. *Biophys. J.* 80:278a. (Abstr.)

Coudrier, E., D. Kerjaschki, and D. Louvard. 1988. Cytoskeleton organization and submembranous interactions in intestinal and renal brush borders. *Kidney Int.* 34:309–320.

Cremo, C. R., and M. A. Geeves. 1998. Interaction of actin and ADP with the head domain of smooth muscle myosin: implications for strain-dependent ADP release in smooth muscle. *Biochemistry.* 37:1969–1978.

Durrbach, A., K. Collins, P. Matsudaira, D. Louvard, and E. Coudrier. 1996. Brush border myosin-I truncated in the motor domain impairs the distribution and the function of endocytic compartments in a hepatoma cell line. *Proc. Natl. Acad. Sci. U.S.A.* 93:7053–7058.

Durrbach, A., G. Raposo, D. Tenza, D. Louvard, and E. Coudrier. 2000. Truncated brush border myosin I affects membrane traffic in polarized epithelial cells. *Traffic.* 1:411–24.

Fath, K. R., and D. R. Burgess. 1994. Membrane motility mediated by unconventional myosin. *Curr. Opin. Cell Biol.* 6:131–135.

Harris, D. E., and D. M. Warshaw. 1993. Smooth and skeletal muscle myosin both exhibit low duty cycles at zero load in vitro. *J. Biol. Chem.* 268:14764–14768.

Hasson, T., and M. S. Mooseker. 1994. Porcine myosin VI: characterization of a new mammalian unconventional myosin. *J. Cell Biol.* 127: 425–440.

Heintzelman, M., T. Hasson, and M. Mooseker. 1994. Multiple unconventional myosin domains of the intestinal brush border cytoskeleton. *J. Cell Sci.* 107:3535–3543.

Heintzelman, M. B., and M. S. Mooseker. 1990. Assembly of the brush border cytoskeleton: changes in the distribution of microvillar core proteins during enterocyte differentiation in adult chicken intestine. *Cell Motil. Cytoskel.* 15:12–22.

Hirschberg, K., C. M. Miller, J. Ellenberg, J. F. Presley, E. D. Siggia, R. D. Phair, and J. Lippincott-Schwartz. 1998. Kinetic analysis of secretory protein traffic and characterization of golgi to plasma membrane transport intermediates in living cells. *J Cell Biol.* 143:1485–503.

Howard, J. 2001. Mechanics of Motor Proteins and the Cytoskeleton. Sinauer Associates, New York.

Jontes, J. D., and R. A. Milligan. 1997. Brush border myosin-I structure and ADP-dependent conformational changes revealed by cryoelectron microscopy and image analysis. *J. Cell Biol.* 139:683–693.

Jontes, J. D., R. A. Milligan, T. D. Pollard, and E. M. Ostap. 1997. Kinetic characterization of brush border myosin-I ATPase. *Proc. Natl. Acad. Sci. U.S.A.* 94:14332–14337.

Jontes, J. D., E. M. Wilson-Kubalek, and R. A. Milligan. 1995. A 32 degree tail swing in brush border myosin I on ADP release. *Nature.* 378: 751–753.

Kenny, A. J., and A. G. Booth. 1978. Microvilli: their ultrastructure, enzymology and molecular organization. *Essays Biochem.* 14:1–44.

Luby-Phelps, K., P. E. Castle, D. L. Taylor, and F. Lanni. 1987. Hindered diffusion of inert tracer particles in the cytoplasm of mouse 3T3 cells. *Proc. Natl. Acad. Sci. U.S.A.* 84:4910–4913.

Mooseker, M. S. 1985. Organization, chemistry, and assembly of the cytoskeletal apparatus of the intestinal brush border. *Annu. Rev. Cell Biol.* 1:209–241.

Mooseker, M. S., and R. E. Cheney. 1995. Unconventional myosins. *Annu. Rev. Cell Dev. Biol.* 11:633–675.

Mooseker, M. S., and C. L. Howe. 1982. The brush border of intestinal epithelium: a model system for analysis of cell-surface architecture and motility. *Methods Cell Biol.* 25:143–174.

Nehls, S., E. L. Snapp, N. B. Cole, K. J. Zaal, A. K. Kenworthy, T. H. Roberts, J. Ellenberg, J. F. Presley, E. Siggia, and J. Lippincott-Schwartz. 2000. Dynamics and retention of misfolded proteins in native ER membranes. *Nat. Cell Biol.* 2:288–295.

Peterson, M. D., W. M. Bement, and M. S. Mooseker. 1993. An in vitro model for the analysis of intestinal brush border assembly. II. Changes in expression and localization of brush border proteins during cell contact-induced brush border assembly in Caco-2BBe cells. *J. Cell Sci.* 105:461–472.

Peterson, M. D., and M. S. Mooseker. 1992. Characterization of the enterocyte-like brush border cytoskeleton of the C2BBe clones of the human intestinal cell line, Caco-2. *J. Cell Sci.* 102:581–600.

Peterson, M. D., and M. S. Mooseker. 1993. An in vitro model for the analysis of intestinal brush border assembly. I. Ultrastructural analysis of cell contact-induced brush border assembly in Caco-2BBe cells. *J. Cell Sci.* 105:445–460.

Pollard, T. D., and M. S. Mooseker. 1981. Direct measurement of actin polymerization rate constants by electron microscopy of actin filaments nucleated by isolated microvillus cores. *J. Cell Biol.* 88:654–659.

Raposo, G., M. N. Cordonnier, D. Tenza, B. Menichi, A. Durrbach, D. Louvard, and E. Coudrier. 1999. Association of myosin I alpha with endosomes and lysosomes in mammalian cells. *Mol. Biol. Cell.* 10: 1477–1494.

Ruppert, C., J. Godel, R. T. Muller, R. Kroschewski, J. Reinhard, and M. Bahler. 1995. Localization of the rat myosin I molecules myr 1 and myr 2 and in vivo targeting of their tail domains. *J. Cell Sci.* 108:3775–3786.

Sacks, D. B., S. E. Porter, J. H. Ladenson, and J. M. McDonald. 1991. Monoclonal antibody to calmodulin: development, characterization, and comparison with polyclonal anti-calmodulin antibodies. *Anal. Biochem.* 194:369–677.

Skowron, J. F., W. M. Bement, and M. S. Mooseker. 1998. Human brush border myosin-I and myosin-Ic expression in human intestine and Caco-2BBe cells. *Cell Motil. Cytoskel.* 41:308–324.

Stidwill, R. P., and D. R. Burgess. 1986. Regulation of intestinal brush border microvillus length during development by the G- to F-actin ratio. *Dev. Biol.* 114:381–388.

Stidwill, R. P., T. Wysolmerski, and D. R. Burgess. 1984. The brush border cytoskeleton is not static: in vivo turnover of proteins. *J. Cell Biol.* 98:641–645.

Tang, N., and E. M. Ostap. 2001. Motor domain-dependent localization of myo1b (myr-1). *Curr Biol.* 11:1131–1135.

Veigel, C., L. M. Coluccio, J. D. Jontes, J. C. Sparrow, R. A. Milligan, and J. E. Molloy. 1999. The motor protein myosin-I produces its working stroke in two steps. *Nature.* 398:530–533.

Wolenski, J. S., S. M. Hayden, P. Forscher, and M. S. Mooseker. 1993. Calcium-calmodulin and regulation of brush border myosin-I MgATPase and mechanochemistry. *J. Cell Biol.* 122:613–621.